Low Retention of [*S-methyl*-^{11}C]MeS-IMPY to β-amyloid Plaques in Patients with Alzheimer's Disease

Nicholas Seneca[a,*], Lisheng Cai[a], Jeih-San Liow[a], Sami S. Zoghbi[a], Robert Gladding[a], John T. Little[b], Paul S. Aisen[b], Jinsoo Hong[a], Victor W. Pike[a] and Robert B. Innis[a]

[a]*Molecular Imaging Branch, National Institute of Mental Health, Bethesda, MD,USA;* [b]*Memory Disorders Program, Department of Neurology, Georgetown University Medical Center, Washington DC, USA*

Abstract: Alzheimer's disease (AD) is characterized pathologically by the accumulation of β-amyloid plaques in brain. We developed a novel positron emission tomographic (PET) radioligand, [^{11}C]MeS-IMPY ([*S-methyl*-^{11}C]*N*,*N*-dimethyl-4-(6-(methylthio)imidazo[1,2-*a*]pyridine-2-yl)aniline). The objective of this study was to determine if [^{11}C]MeS-IMPY can detect β-amyloid plaques in patients with AD. Ten subjects (4 patients with AD and 6 healthy controls) had PET scans of 90 min as well as serial sampling of arterial plasma. Total distribution volume was calculated from radioactivity in brain and concentrations of radioligand in arterial plasma. After injection of [^{11}C]MeS-IMPY in both groups, peak brain uptake was high (~ 450% SUV), peaked early at ~ 2 min and washed out quickly. The time-course of brain radioactivity in all regions was virtually identical in AD patients and healthy controls. Although distribution volume of neocortical regions was ~ 26% higher in AD patients than in controls, the differences were statistically insignificant (P = 0.143). In addition, distribution volume in all regions and in both groups increased during the entire scan, which is consistent with the accumulation of radiometabolite(s) in brain. The rapid washout of [^{11}C]MeS-IMPY from brain may have been caused by inadequate binding affinity, and the small differences between patients and healthy subjects were likely caused, in part, by the accumulation of radiometabolite(s) in brain. We conclude that [^{11}C]MeS-IMPY is able to image β-amyloid in brains of patients with AD, but that chemical analogs with higher affinity and non-problematic radiometabolites will be more useful imaging agents.

Key Words: Positron emission tomography, β-amyloid, [^{11}C]MeS-IMPY, Alzheimer's disease.

INTRODUCTION

Brain imaging studies using PET radioligands such as [^{11}C]PIB, [^{18}F]FDDNP, [^{11}C]SB-13, and [^{18}F]BAY94-9172, have demonstrated the feasibility to image β-amyloid in patients with AD [1-4]. Since accumulation of β-amyloid has been proposed as one of the underlying pathophysiologies of AD, *in vivo* quantification of β-amyloid may provide a useful tool to diagnose the disease, to monitor novel therapeutics, and to explore the role of β-amyloid plaques in the disease. Thus, several PET radioligands have recently been developed to image β-amyloid and are reviewed elsewhere [5,6].

MeS-IMPY binds selectively and with moderately high affinity (K_i = 7.93 nM) to human β-amyloid plaques in postmortem brain tissue of patients with AD [7]. [*S-methyl*-^{11}C]MeS-IMPY ([^{11}C]MeS-IMPY) showed promising *in vivo* characteristics in rodent and monkey brain as a potential radioligand for imaging β-amyloid plaques [7,8]. [^{11}C]MeS-IMPY showed high brain uptake and rapid washout, widespread distribution to all cortical regions, slightly higher values of distribution volume in white compared to grey matter, and stable measurements of distribution volume using one-tissue compartmental analysis [8]. In addition, whole-body PET imaging of [^{11}C]MeS-IMPY caused moderate to low radiation exposure, which would allow multiple PET scans per year in the same subject. These promising *in vitro* and *in vivo* characteristics made this PET radioligand a potential probe to image β-amyloid plaques in patients with AD. The purpose of this study was to determine if [^{11}C]MeS-IMPY can detect β-amyloid plaques in patients with AD.

*Address correspondence to this author at National Institute of Mental Health, Molecular Imaging Branch, Bldg. 31, Room B2B34; MSC-2035, Bethesda, MD 20892-2035, USA; Tel: (301) 594-1089; Fax: (301) 480-3610; E-mail: NICHOLAS.SENECA@ROCHE.COM

METHODS

Radioligand Preparation

[^{11}C]MeS-IMPY was prepared as previously described, namely by ^{11}C-*S*-methylation of methyl 3-(2-(4-(dimethylamino)phenyl)imidazo[1,2-*a*]pyridin-6-ylthio)propanoate [7]. Preparations were conducted according to our Investigational New Drug Application #76,568, submitted to the US Food and Drug Administration, and a copy of which is available at: http://pdsp.med.unc.edu/snidd/. The radioligand was obtained in high radiochemical purity (~ 99%) and with specific activity at time of injection of 52 ± 16 GBq/μmol (n = 10 batches).

Human Subjects

Four patients with AD (2 females and 2 males) and six healthy subjects (6 males) participated. All AD patients met NINCDS-ADRDA criteria for probable AD and scored between 24 and 28 on the Mini-Mental Status Examination (MMSE). The average number of years of diagnosis for all four patients was three. AD patients ranged in age from 60 to 75 with a mean age of 70. Healthy subjects were free of cur-

1874-4710/09 $55.00+.00

rent medical and psychiatric illness based on history, physical examination, electrocardiogram, and urinalysis including drug screening, blood tests (complete blood count, serum chemistries, thyroid function test, and antibody screening for syphilis, HIV, and hepatitis B) and scored between 28 and 30 on the MMSE. Healthy subjects included 2 young and 4 age-matched controls with a mean age of 23 and 63 y, respectively. Healthy controls, young plus old were pooled together. All subjects returned to repeat urinalysis and blood tests about 24 h after the PET scan.

PET Studies

After injection of [^{11}C]MeS-IMPY (650 ± 131 MBq) in the ten subjects, PET scans were acquired for 90 min in 27 frames. All PET scans were performed on a GE Advance PET camera. Images were acquired in the axial orientation with respect to the subject. Each emission scan consisted of a dynamic acquisition with frame schedule of 30 s from 0 – 180 s, 1 min from 3 – 6 min, 2 min from 6 – 10 min, and 5 min from 10 – 90 min. All PET images were corrected for attenuation and scatter. The subjects' vital signs were recorded before [^{11}C]MeS-IMPY injection and at 15, 30, and 90 min after injection.

Magnetic Resonance Imaging

To identify brain regions, T 1 weighted magnetic resonance imaging (MRI) scans of 1.2 mm contiguous slices were obtained with a GE Signa 1.5 T scanner. Three sets of axial images were acquired with a spoiled GRASS (gradient recall acquisition in the steady state) sequence with TR = 12.4 ms, TE = 5.3 ms, flip angle = 20°, and matrix = 256×256.

Measurement of [^{11}C]MeS-IMPY in Plasma

Blood samples (1 mL each) were drawn from the radial artery at 15 s intervals until 120 s, followed by 2 mL samples at 3, 5, 8, and 10 min, and 3 mL samples at 15, 20, 30, 40, 55, 70, and 85 min. The plasma time-activity curve was corrected for the fraction of unchanged radioligand, as previously described [9].

The free fraction of [^{11}C]MeS-IMPY in plasma was measured by ultrafiltration through Centrifree membrane filters (Amicon Division, W.R. Grace and Co., Danvers, MA, USA) as previously described [10]. Plasma samples from each subject were stored in a –70° C freezer and free fractions were measured on a day other than the PET scan. Measurements were performed twice with all plasma samples receiving a common preparation of [^{11}C]MeS-IMPY each time.

Image Analysis

All MRI and PET images were spatially normalized to a standard anatomic template in Montreal Neurological Institute (MNI) space. The spatial normalization was consolidated into a single computer script which utilized a mutual information based coregistration in the FMRIB Software Library (FMRIB Analysis Group, Oxford, UK) and is described as follows. First, a summed PET image of all time frames was coregistered to the MRI of the individual subject using a 6-parameter algorithm. Second, the individual's MRI was coregistered to the template MRI in MNI space using a 12-parameter algorithm. The transformation from the PET to subject MRI and from the subject MRI to template MRI were then combined and applied to resample the individual's dynamic PET image into the MNI space. The PET images after resampling were visually inspected for every time-frame with respect to the MNI template to ensure a good match.

Transforming PET images into the MNI space allowed the application of Automated Anatomical Labeling map (AAL) [11], which consists of 116 brain regions defined in the MNI space. Using a set of standardized regions of interest across all subjects provided greater objectivity, consistent region size, and better reproducibility of results. After obtaining their means, we condensed the 116 regions by pixel-weighted averaging to 8 regions, comprised of the prefrontal, frontal, parietal, occipital, lateral temporal, medial temporal, posterior cingulate cortices, and cerebellum. One additional region of interest in the white matter was hand drawn on the MNI template, confirmed by fellow investigators and added to the region of interest set. Time-activity curves were constructed for the 9 regions and evaluated. We applied an atrophy correction to the PET data by segmenting each individual's T1 weighted MRI scan into a binary grey, white and CSF (cerebrospinal fluid) compartment, transforming the grey matter volume into MNI space following coregistration information between the individual and template MRI, and finally, applying the AAL template to the transformed gray matter volume to calculate a grey matter fraction for each region. These fractions were used as scale factors to adjust the region means obtained from the PET image. The average grey matter fractions across all regions for healthy controls was 0.85 and for AD patients was 0.81. Time-activity curves were expressed as a standardized uptake value (%SUV), which normalizes for injected activity and body weight: (% injected activity/cm^3 tissue) × (g body weight). Image and kinetic analyses were performed using PMOD 2.85 (pixel-wise modeling software; PMOD Technologies Ltd., Zurich, Switzerland) [12].

Calculation of Distribution Volume and Reference Tissue Model

Distribution volume is a measure of receptor density and is equal to the ratio at equilibrium of the concentration of radioligand in tissue to that in plasma. Total distribution volume V_T includes the concentrations of all radioligand in tissue, which is composed of specific (*i.e.*, receptor bound) and nondisplaceable (*i.e.*, nonspecifically bound and free radioligand in tissue water). The equilibrium value of V_T was calculated from measurements over time of radioactivity in brain and of the concentrations of radioligand in arterial plasma. The serial concentrations of radioligand in plasma are referred to as the "input function." The input function was analyzed as linear interpolation of the concentrations of [^{11}C]MeS-IMPY before the peak, and a bi-exponential fit of concentrations after the peak. The concentration of [^{11}C]MeS-IMPY separated from radiometabolites was used as the sole input function. Rate constants (K_1, k_2, k_3, and k_4) in standard one- and two-tissue compartment models [13] were calculated with weighted least squares and the Marquardt optimizer. Brain data of each frame were weighted by

assuming that the standard deviation of the data is proportional to the inverse square root of noise equivalent counts. To correct the brain data for its vascular component, radioactivity in serial whole blood was measured and then subtracted from the PET measurements assuming that cerebral blood volume is 5% of total brain volume.

To determine the minimum scanning time necessary to obtain stable values of distribution volume, we analyzed the PET data from each subject after removing variable durations of the terminal portion of the scan. We analyzed brain data of all subjects from 0 – 30 min to 0 – 90 min, with 10-min increments.

In addition, we analyzed the brain PET data using the Logan graphical analysis model [14]. The cerebellum was used as the reference region, which has been shown to contain negligible densities of β-amyloid [15].

Statistical Analysis

Goodness-of-fit by nonlinear least squares analysis was evaluated with the Akaike Information Criterion (AIC) [16]. The most appropriate model has the smallest AIC. Goodness-of-fit by the compartmental models was compared with *F* statistics. This analysis was performed for all regions of interest and a value of $P < 0.05$ was considered significant for *F* statistics.

The identifiability of the kinetic variables was calculated by the compartmental fitting as the standard error, which itself reflects the diagonal of the covariance matrix [17]. Identifiability is expressed as a percentage and equals the ratio of the standard error of the rate constant divided by the value of the rate constant itself. Identifiability of V_T was calculated from the covariance matrix using the generalized form of error propagation equation [18], where correlations among the rate constants were taken into account.

Data are expressed as mean ± SD. A comparison of the total distribution volume and reference tissue model between healthy controls and AD patients was assessed using an ANOVA. All statistical analysis was performed with healthy control subjects (young plus old) *vs.* AD and healthy control subjects (old age-matched) *vs.* AD. Differences between groups cerebellar uptake and concentrations of [11C]MeS-IMPY in plasma were compared using a Linear mixed model with heterogeneous first-order autoregressive covariant structure. Bonferroni post-hoc tests compared the two groups to determine any differences between the groups. The minimum level of significance was designated as $P < 0.05$. All statistical analyses were performed using SPSS version 15.

RESULTS

After injection of [11C]MeS-IMPY, the mean magnitudes and time courses of brain radioactivity in all regions, except cerebellum, were virtually identical in AD patients and healthy controls Figs. (**1** and **2**). The peak brain uptake was high (~ 450% SUV) in both groups, peaked early at ~ 2 min, and washed out quickly Fig. (**1**). The mean uptake in cerebellum was slightly lower in AD patients than in healthy controls. Although small, this difference in cerebellar curves was statistically significant ($P = 0.036$) during time frames 37.5 to 62.5 min of the entire 90 min of scanning. Statistical

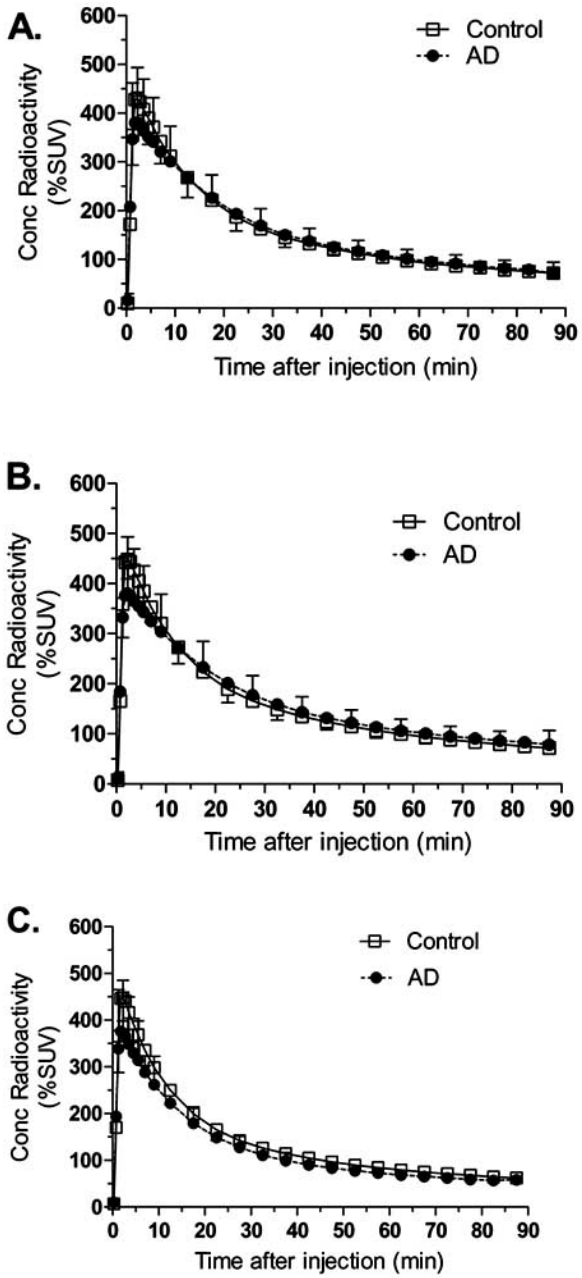

Fig. (1). Time-activity curves of [11C]MeS-IMPY in healthy controls ($n = 6$) and patients with Alzheimer's disease ($n = 4$). Concentrations of radioactivity in medial (**A**) and lateral (**B**) temporal cortex and cerebellum (**C**) after injection of [11C]MeS-IMPY. Symbols represent the mean ± SD, although the SD is sometimes less than the size of the symbol. The SD bars are shown for every other value and alternate between the healthy controls and Alzheimer's disease patients.

significance remained the same for all PET outcome measures whether AD patients were compared with all healthy subjects (young and old) or with only the old healthy subjects. Furthermore, since the young and old healthy controls were not significantly different, subsequent analyses combined both the two young and four old healthy subjects into a single control group ($n = 6$).

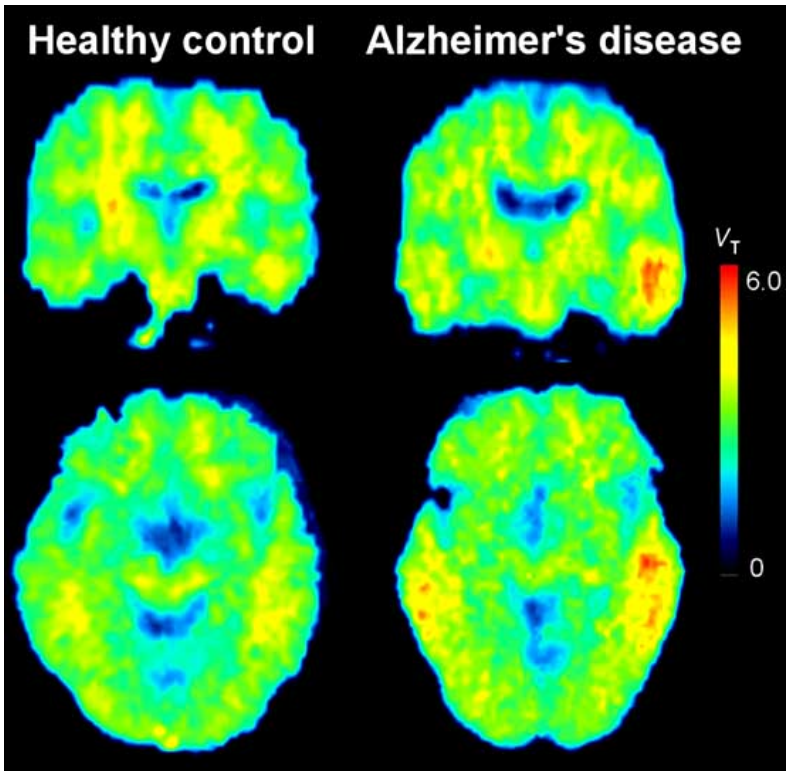

Fig. (2). PET images of [^{11}C]MeS-IMPY calculated by distribution volume in healthy control (left) and Alzheimer's disease patient (right). Alzheimer's disease patients had slightly higher retention of [^{11}C]MeS-IMPY in neocortical areas compared to healthy controls. Each image is a representative sample for the six healthy controls and three of the four Alzheimer's disease patients.

The concentration of [^{11}C]MeS-IMPY in plasma peaked at 1 min after the start of a bolus injection, which was administered with a pump and lasted for 1 min. The concentrations after this peak were well fit with a biexponential function and had mean half lives in healthy controls of 0.5 and 14 min, compared to AD patients of 0.4 and 10 min (Table **1**). Calculated as the partial areas under the concentration *vs.* time curve, these two half-lives accounted for 35% and 65% for healthy controls and 32% and 68% for AD patients of the total area under the curve from peak to infinity (Table **1**). The total AUC was ~ 10% higher for the healthy controls compared to AD patients (Table **1**).

The fraction of [^{11}C]MeS-IMPY, expressed as a percentage of total plasma activity, declined relatively quickly and reached 50% at ~ 8 min in both groups Fig. (**3A**). The three radiometabolite peaks A-C eluted prior to MeS-IMPY Fig. (**3B**) and were therefore less lipophilic than MeS-IMPY. The plasma free fraction (f_p) of [^{11}C]MeS-IMPY in AD patients (0.85%) was half that in healthy controls (1.7%) (P = 0.034). Since only the radioligand that is unbound to plasma proteins is available for diffusion across the blood-brain barrier, correcting for any differences in f_p between the groups may be the more appropriate measure of radioligand binding to amyloid. However, correcting for plasma free fraction (*i.e.*, V_T/f_p) would have an equal effect on all brain regions and would not change the ratio of target to background region (*e.g.*, neocortex to cerebellum).

Distribution volume was calculated using compartmental modeling of time-activity brain data and the serial concentrations of [^{11}C]MeS-IMPY in arterial plasma. For all subjects and brain regions, the two-tissue compartmental model provided significantly better fit than the one-tissue compartmental model (F-test, $P < 0.001$) Fig. (**4A**) and had low AIC (116 ± 24) and high MSC (4 ± 1) scores. Using results from the two-tissue compartmental model, even though some of the individual rate constants (K_1, k_2, k_3, k_4) were poorly identified, total distribution volume (V_T) had good identifiability (<10%) in all regions for both AD patients and healthy con-

Table 1. Pharmacokinetic Parameters of [^{11}C]MeS-IMPY in Plasma Between Two Groups

	Half-Lives (min)		AUC of Exponential as % Total AUC		Total AUC (kBq/mL · min)	
	Healthy Controls	Alzheimer's Disease	Healthy Controls	Alzheimer's Disease	Healthy Controls	Alzheimer's Disease
Exponential (1)	0.46 ± 0.17	0.38 ± 0.05	35% ± 6	32% ± 12	279 ± 60	254 ± 39
Exponential (2)	14.15 ± 9.08	9.66 ± 3.95	65% ± 6	68% ± 12		

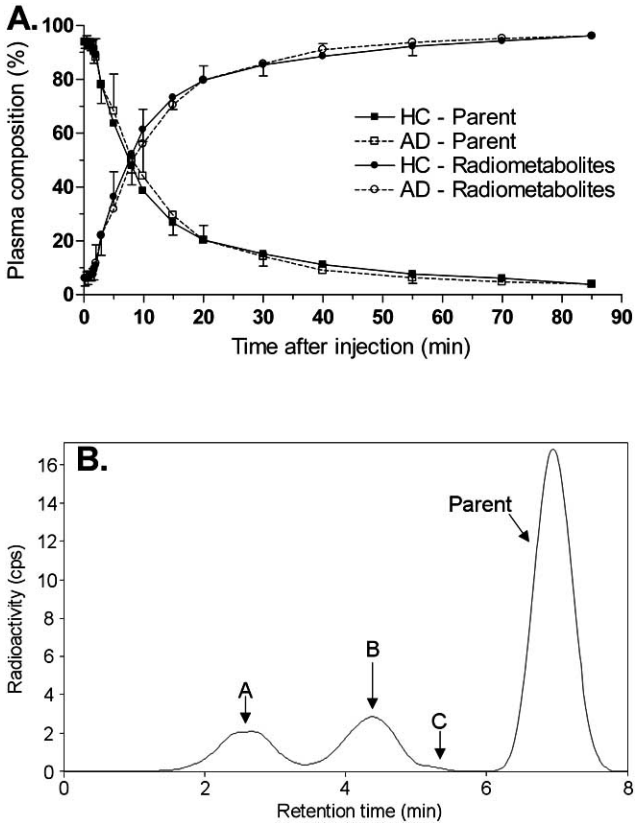

Fig. (3). (**A**) The percentage composition of plasma radioactivity over time is shown for [11C]MeS-IMPY and total radiometabolites. Symbols represent the mean ± SD, although the SD is sometimes less than the size of the symbol. The SD bars are shown for every other value and alternate between the healthy controls and Alzheimer's disease patients. (**B**) Radiochromatogram of plasma from a healthy control subject at 5 min after injection of [11C]MeS-IMPY. Parent constituted 70% of total radioactivity. Radiometabolites (A-C) have lower lipophilicity than that of [11C]MeS-IMPY.

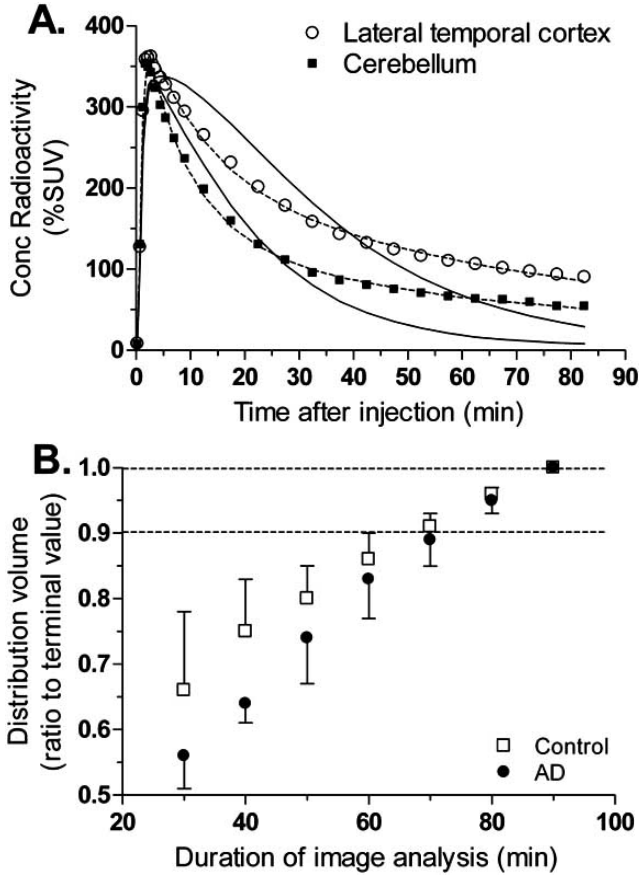

Fig. (4). Compartmental modeling of dynamic PET images. (**A**) The two-tissue compartmental model (dashed lines) more closely followed the measured values of the lateral temporal cortex (○) and cerebellum (■) than did the one-tissue compartmental model (solid lines). (**B**) Time stability of V_T determined from the two-tissue compartmental model was assessed by analyzing increasingly truncated data, with a range of 0-30 min to 0-90 min, as above. Each point represents the average V_T in nine regions of interest in healthy controls (□) and Alzheimer's disease patients (●) with data from time 0 to the specified time and expressed as the percentage of the 90-min value.

trols. Although distribution volume of the neocortical regions was ~ 26 % higher in AD patients than in healthy controls, the differences were statistically insignificant Figs. (**2** and **5**) (P = 0.143). The increase in V_T was similar using atrophy corrected or raw PET data.

The time stability of V_T was analyzed for all regions using the two-tissue compartmental model. V_T in all regions and in both groups continuously increased during the scan Fig. (**4B**). The gradual increase in V_T is consistent with a possible accumulation of radiometabolite(s) in brain, which thereby impairs the accuracy of compartmental modeling to quantify V_T.

Quantification with a reference tissue model demonstrated statistically significant group differences in the retention of [11C]MeS-IMPY in several brain regions known to contain high densities of β-amyloid such as frontal (P = 0.48), lateral temporal (P = 0.14), parietal (P = 0.10) and prefrontal cortices (P = 0.18) Fig. (**6**). However, after controlling for differences in cerebellar uptake, no significant differences were detected between healthy control subjects and AD patients. Thus, the significant differences found with the reference tissue model were due merely to differences in cerebellar uptake. Furthermore, since cerebellum contains negligible amounts of amyloid, these differences have no relation to the retention of radioligand by amyloid.

DISCUSSION

The purpose of this study was to determine whether [11C]MeS-IMPY has greater retention in brains of patients with AD compared to those of healthy controls, who would likely have little β-amyloid in brain. We found that [11C]MeS-IMPY has low retention (~ 12% increase of PET outcome measure) in brain regions known to contain high densities of β-amyloid plaques in patients with AD. This moderate to low increase in the PET outcome measure is similar to that of other PET radioligands such as [18F]FDDNP (~ 9%) and [11C]BF-227 (~ 12%) (Table **2**).

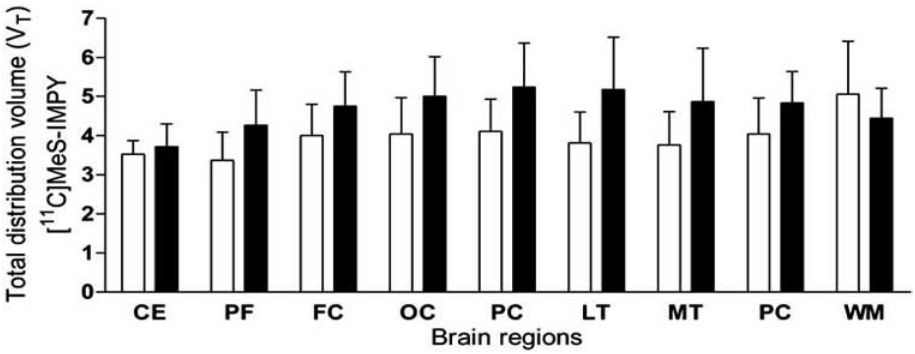

Fig. (5). No statistical significant differences in the total distribution volume (V_T) between AD patients (closed bars) and healthy controls (open bars) (P = 0.219). CE = cerebellum, PF = prefrontal cortex, FC = frontal cortex, OC = occipital cortex, PC = parietal cortex, LT = lateral temporal cortex, MT = medial temporal cortex, PC = posterior cingulate gyrus, and WM = white matter.

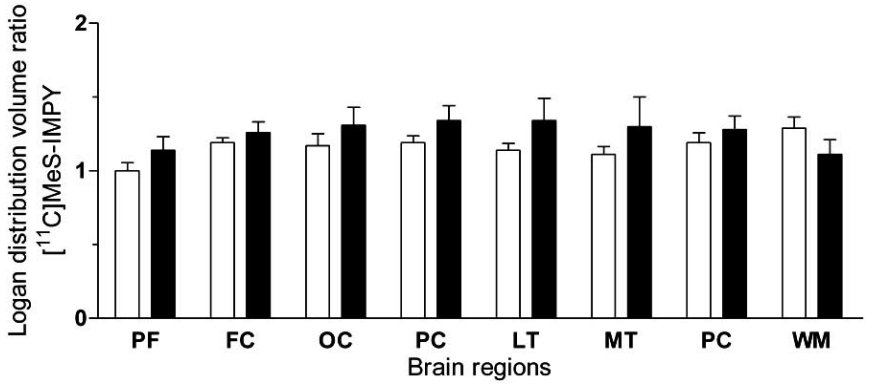

Fig. (6). Statistical significant differences in regions known to contain high densities of β-amyloid between AD patients (closed bars) and healthy controls (open bars) calculated using the Logan distribution volume ratio. CE = cerebellum, PF = prefrontal cortex (P = 0.18), FC = frontal cortex (P = 0.48), OC = occipital cortex, PC = parietal cortex (P = 0.10), LT = lateral temporal cortex (P = 0.14), MT = medial temporal cortex, PC = posterior cingulate gyrus, and WM = white matter.

The low retention to β-amyloid plaques in AD patients using [^{11}C]MeS-IMPY was surprising since its *in vitro* characteristics are similar to those of other successful PET radioligands (Table **2**). Although a comparison of affinity, brain uptake, and lipophilicity may not be strictly accurate because of differing assay conditions, the values for [^{11}C]MeS-IMPY are in range of a few successful PET radioligands to image β-amyloid plaques. The reasons for the low retention of [^{11}C]MeS-IMPY in brains of AD patients remain unclear, but we suggest three possibilities. First, [^{11}C]MeS-IMPY has only moderate binding affinity (K_i = 7.9 nM) for β-amyloid [7]. Despite the high abundance of binding sites on amyloid plaques, the affinity of this radioligand may be too low to have significant retention. Second, the patients in this study may have had relatively small amounts of β-amyloid in brain. Their MMSE scores (mean = 26) were higher than those in four other studies (mean = 20−24) that used radioligands for β-amyloid [3,19-21]. Third, radiometabolites of [^{11}C]MeS-IMPY in brain may have increased the nonspecific signal such that the specific signal (*i.e.*, parent radioligand binding to β-amyloid) could not be detected.

Among the three possibilities, we suspect that metabolism of the radioligand may be the most problematic. Three radiometabolite peaks (A−C) were detected with HPLC analysis in rodent, monkey and human plasma [7,8]. Across these species, the three radiometabolites were relatively less lipophilic than the parent radioligand but still had adequate lipophilicity to enter brain. For example, the $LogD_{7.4}$ of [^{11}C]MeS-IMPY is 4.1, whereas that of its predominant radiometabolite (B) is 3.6 [7]. The lipophilicity of this radiometabolite is well within the range (~ 1− 5) of brain-penetrant compounds. After injection of [^{11}C]MeS-IMPY, ~ 70% of the total radioactivity in rat brain at 3 min was composed of radiometabolites [7]. Using liquid chromatography-mass spectrometry (LC-MS) and tandem mass spectrometry (MS-MS), we identified the major radiometabolite in rat brain to be [^{11}C]*N-desmethyl*-MeS-IMPY. Furthermore, [^{11}C]MeS-IMPY was metabolized in rat brain homogenates (~ 7% after 60 min incubation), suggesting that this radiometabolite may not only pass the blood-brain barrier but also be generated in the brain itself. The similarities between the plasma radiochromatograms across species imply the generation of a similar spectrum of radiometabolites and that *N*-demethylation is the primary route of metabolism. Rapid accumulation of three radiometabolites (~ 50% of plasma composition by 10 min) in human arterial plasma samples may have led to the accumulation of one or more of these radiometabolites in human brain Fig. (**3**). Our results support this possibility, since the estimation of V_T did not stabilize but increased during the entire scan Fig. (**4B**), consistent with the accumulation of radiometabolites in human brain.

Table 2. Structure, Affinity, Peak Brain Uptake, Lipophilcity, and % Increase of PET Outcome Measure of Seven Radioligands used for Imaging β-amyloid Plaques in Patients with AD

Radioligand	Structure	K_i (nM)	Brain Peak (%SUV)	Lipophilicity ($LogD_{7.4}$)	% Increase of PET Measure AD *vs* HC
[^{18}F]FDDNP[1,21]	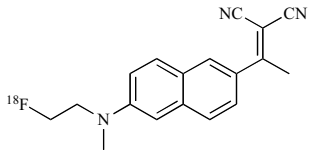	0.12[1]	—	3.92[1]	9[21]
[^{11}C]MeS-IMPY[7]	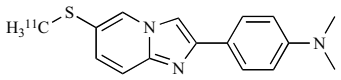	7.93[7]	450	4.1[7]	12
[^{11}C]BF-227[19]	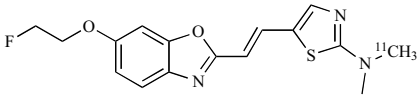	4.3[19]	300	1.75[19]	12[19]
[^{123}I]IMPY[22]	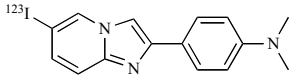	8.95[5]	—	3.58[5]	44[22]
[^{11}C]SB-13[4]	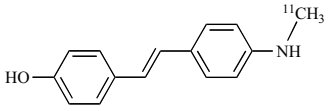	2.4[23]	500	2.36[23]	55[4]
[^{18}F]BAY94-9172[3]	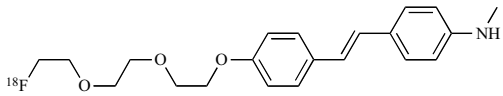	6.7[24]	400	2.41[24]	57[3]
[^{11}C]PIB[2]	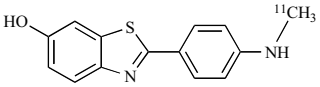	4.3[25]	400	1.3[25]	130

In summary, the PET radioligand [^{11}C]MeS-IMPY showed high brain uptake, plasma concentrations of parent peaked quickly and declined rapidly, three radiometabolites in plasma were less lipophilic than MeS-IMPY, and total distribution volume (V_T) had good identifiability. However, [^{11}C]MeS-IMPY (12% increase compared to healthy controls) lacked binding comparable to the "gold standard" [^{11}C]PIB (130% increase compared to healthy controls) to β-amyloid plaques in patients with AD. The unexpected results may have been due to several factors, including inadequate binding affinity, mild severity of symptoms in these AD patients and an associated small amount of β-amyloid in brain, or the accumulation of radiometabolites in brain.

ACKNOWLEDGEMENTS

The authors thank Edward Tuan and Pavitra Kannan for assistance with the arterial blood samples; the staff of the NIH PET department for successful completion of the scanning studies; and PMOD Technologies, Ltd. (Zurich, Switzerland) for providing its image analysis and modeling software. A patent application has been filed on behalf of the US government and could personally benefit VWP, LC, and RBI. This research was supported by the Intramural Program of NIMH (project #Z01-MH-002852-04).

REFERENCES

[1] Agdeppa, E.D.; Kepe, V.; Petri, A.; Satyamurthy, N.; Liu, J.; Huang, S.C.; Small, G.W.; Cole, G.M.; Barrio, J.R. *In vitro* detection of (*S*)-naproxen and ibuprofen binding to plaques in the Alzheimer's brain using the positron emission tomography molecular imaging probe 2-(1-[6-[(2-[^{18}F]fluoroethyl)(methyl)amino]-2-naphthyl]ethylidene)malono nitrile. *Neuroscience*, **2003**, *117*, 723-30.

[2] Klunk, W.E.; Engler, H.; Nordberg, A.; Wang, Y.; Blomqvist, G.; Holt, D.P.; Bergstrom, M.; Savitcheva, I.; Huang, G.F.; Estrada, S.; Ausen, B.; Debnath, M.L.; Barletta, J.; Price, J.C.; Sandell, J.; Lopresti, B.J.; Wall, A.; Koivisto, P.; Antoni, G.; Mathis, C.A.; Långström, B. Imaging brain amyloid in Alzheimer's disease with Pittsburgh Compound-B. *Ann. Neurol.*, **2004**, *55*, 306-19.

[3] Rowe, C.C.; Ackerman, U.; Browne, W.; Mulligan, R.; Pike, K.L.; O'Keefe, G.; Tochon-Danguy, H.; Chan, G.; Berlangieri, S.U.;

Jones, G.; Dickinson-Rowe, K.L.; Kung, H.P.; Zhang, W.; Kung, M.P.; Skovronsky, D.; Dyrks, T.; Holl, G.; Krause, S.; Friebe, M.; Lehman, L.; Lindemann, S.; Dinkelborg, L.M.; Masters, C.L.; Villemagne, V.L. Imaging of amyloid beta in Alzheimer's disease with ^{18}F-BAY94-9172, a novel PET tracer: proof of mechanism. *Lancet Neurol.*, **2008**, *7*, 129-35.

[4] Verhoeff, N.P.; Wilson, A.A.; Takeshita, S.; Trop, L.; Hussey, D.; Singh, K.; Kung, H.F.; Kung, M.P.; Houle, S. *In vivo* imaging of Alzheimer disease beta-amyloid with [^{11}C]SB-13 PET. *Am. J. Geriatr. Psychiatry*, **2004**, *12*, 584-95.

[5] Cai, L.; Innis, R.B.; Pike, V.W. Radioligand development for PET imaging of beta-amyloid (A_β)--current status. *Curr. Med. Chem.*, **2007**, *14*, 19-52.

[6] Lockhart, A. Imaging Alzheimer's disease pathology: one target, many ligands. *Drug Discov. Today*, **2006**, *11*, 1093-9.

[7] Cai, L.; Liow, J.S.; Zoghbi, S.S.; Cuevas, J.; Baetas, C.; Hong, J.; Shetty, H.U.; Seneca, N.M.; Brown, A.K.; Gladding, R.; Temme, S.S.; Herman, M.M.; Innis, R.B.; Pike, V.W. Synthesis and evaluation of *N*-methyl and *S*-methyl ^{11}C-labeled 6-methylthio-2-(4'-N,N-dimethylamino)phenylimidazo[1,2-a]pyridines as radioligands for imaging beta-amyloid plaques in Alzheimer's disease. *J. Med. Chem.*, **2008**, *51*, 148-58.

[8] Seneca, N.; Cai, L.; Liow, J.S.; Zoghbi, S.S.; Gladding, R.L.; Hong, J.; Pike, V.W.; Innis, R.B. Brain and whole-body imaging in nonhuman primates with [^{11}C]MeS-IMPY, a candidate radioligand for beta-amyloid plaques. *Nucl. Med. Biol.*, **2007**, *34*, 681-9.

[9] Zoghbi, S.S.; Shetty, H.U.; Ichise, M.; Fujita, M.; Imaizumi, M.; Liow, J.S.; Shah, J.; Musachio, J.L.; Pike, V.W.; Innis, R.B. PET imaging of the dopamine transporter with ^{18}F-FECNT: a polar radiometabolite confounds brain radioligand measurements. *J. Nucl. Med.*, **2006**, *47*, 520-7.

[10] Gandelman, M.S.; Baldwin, R.M.; Zoghbi, S.S.; Zea-Ponce, Y.; Innis, R.B. Evaluation of ultrafiltration for the free-fraction determination of single photon emission computed tomography (SPECT) radiotracers: beta-CIT, IBF, and iomazenil. *J. Pharm. Sci.*, **1994**, *83*, 1014-9.

[11] Tzourio-Mazoyer, N.; Landeau, B.; Papathanassiou, D.; Crivello, F.; Etard, O.; Delcroix, N.; Mazoyer, B.; Joliot, M. Automated anatomical labeling of activations in SPM using a macroscopic anatomical parcellation of the MNI MRI single-subject brain. *Neuroimage*, **2002**, *15*, 273-89.

[12] Burger, C.; Mikolajczyk, K.; Grodzki, M.; Rudnicki, P.; Szabatin, M.; Buck, A. JAVA tools quantitative post-processing of brain PET data. *J. Nucl. Med.*, **1998**, *39*, 277.

[13] Innis, R.B.; Cunningham, V.J.; Delforge, J.; Fujita, M.; Gjedde, A.; Gunn, R.N.; Holden, J.; Houle, S.; Huang, S.-C.; Ichise, M.; Iida, H.; Ito, H.; Kimura, Y.; Koeppe, R.A.; Knudsen, G.M.; Knuuti, J.; Lammertsma, A.A.; Laruelle, M.; Logan, J.; Maguire, R.P.; Mintun, M.A.; Morris, E.D.; Parsey, R.; Price, J.C.; Slifstein, M.; Sossi, V.; Suhara, T.; Votaw, J.R.; Wong, D.F.; Carson, R.E. Consensus nomenclature for *in vivo* imaging of reversibly binding radioligands. *J. Cereb. Blood Flow. Metab.*, **2007**, *27*, 1533-1539.

[14] Logan, J.; Fowler, J.S.; Volkow, N.D.; Wolf, A.P.; Dewey, S.L.; Schlyer, D.J.; MacGregor, R.R.; Hitzemann, R.; Bendriem, B.; Gatley, S.J.; *et al*. Graphical analysis of reversible radioligand binding from time-activity measurements applied to [*N*-^{11}C-methyl]-(-)-cocaine PET studies in human subjects. *J. Cereb. Blood Flow. Metab.*, **1990**, *10*, 740-7.

[15] Joachim, C.L.; Morris, J.H.; Selkoe, D.J. Diffuse senile plaques occur commonly in the cerebellum in Alzheimer's disease. *Am. J. Pathol.*, **1989**, *135*, 309-19.

[16] Akaike, H. A new look at the statistical model identification. *IEEE Trans. Automat. Control*, **1974**, *AC19*, 716-723.

[17] Carson, R.E. In *Positron Emission Tomography and Autoradiography: Principles and Applications for the Brain and Heart*; Phelps, M. E., Mazziotta, J. C., Schelbert, H. R., Eds.; Raven Press: New York, **1986**, pp. 347-390.

[18] Bevington, P.R.; Robinson, D.K.; McGraw-Hill: New York, **2003**.

[19] Kudo, Y.; Okamura, N.; Furumoto, S.; Tashiro, M.; Furukawa, K.; Maruyama, M.; Itoh, M.; Iwata, R.; Yanai, K.; Arai, H. 2-(2-[2-Dimethylaminothiazol-5-yl]ethenyl)-6- (2-[fluoro]ethoxy)benzoxazole: a novel PET agent for *in vivo* detection of dense amyloid plaques in Alzheimer's disease patients. *J. Nucl. Med.*, **2007**, *48*, 553-61.

[20] Lopresti, B.J.; Klunk, W.E.; Mathis, C.A.; Hoge, J.A.; Ziolko, S.K.; Lu, X.; Meltzer, C.C.; Schimmel, K.; Tsopelas, N.D.; DeKosky, S.T.; Price, J.C. Simplified quantification of Pittsburgh Compound B amyloid imaging PET studies: a comparative analysis. *J. Nucl. Med.*, **2005**, *46*, 1959-72.

[21] Small, G.W.; Kepe, V.; Ercoli, L.M.; Siddarth, P.; Bookheimer, S.Y.; Miller, K.J.; Lavretsky, H.; Burggren, A.C.; Cole, G.M.; Vinters, H.V.; Thompson, P.M.; Huang, S.C.; Satyamurthy, N.; Phelps, M.E.; Barrio, J.R. PET of brain amyloid and tau in mild cognitive impairment. *N. Engl. J. Med.*, **2006**, *355*, 2652-63.

[22] Newberg, A.B.; Wintering, N.A.; Plossl, K.; Hochold, J.; Stabin, M.G.; Watson, M.; Skovronsky, D.; Clark, C.M.; Kung, M.P.; Kung, H.F. Use of ^{123}I-IMPY SPECT to differntiate Alzheimer's disease from controls. *J. Nucl. Med.*, **2006**, *47*, No. 220.

[23] Ono, M.; Wilson, A.; Nobrega, J.; Westaway, D.; Verhoeff, P.; Zhuang, Z.P.; Kung, M.P.; Kung, H.F. ^{11}C-labeled stilbene derivatives as Aβ-aggregate-specific PET imaging agents for Alzheimer's disease. *Nucl. Med. Biol.*, **2003**, *30*, 565-71.

[24] Zhang, W.; Oya, S.; Kung, M.P.; Hou, C.; Maier, D.L.; Kung, H.F. F-18 Polyethyleneglycol stilbenes as PET imaging agents targeting Aβ aggregates in the brain. *Nucl. Med. Biol.*, **2005**, *32*, 799-809.

[25] Mathis, C.A.; Wang, Y.; Holt, D.P.; Huang, G.F.; Debnath, M.L.; Klunk, W.E. Synthesis and evaluation of ^{11}C-labeled 6-substituted 2-arylbenzothiazoles as amyloid imaging agents. *J. Med. Chem.*, **2003**, *46*, 2740-54.

Received: November 04, 2008 Revised: December 02, 2008 Accepted: January 02, 2009